Available online at www.sciencedirect.com
SCIENCE DIRECT®
ELSEVIER
International Journal of Multiphase Flow 30 (2004) 369–393
International Journal of Multiphase Flow
www.elsevier.com/locate/ijmulflow

Surface morphology reconstruction of free falling films at high Reynolds numbers

L.G. Touglidis [a], T.D. Karapantsios [b,*], N.A. Vlachos [b], A.I. Balouktsis [a]

[a] *Technological Educational Institution of Serres, End of Magnesia's str., 62 100 Serres, Greece*
[b] *Department of Chemical Technology, School of Chemistry, Aristotle University, University Box 116, 541 24 Thessaloniki, Greece*

Received 2 June 2003; received in revised form 31 December 2003

Abstract

A novel theoretical treatment is presented for simulating the shape of the wavy surface of thin liquid falling films, flowing freely inside a vertical pipe. The simulation proved particularly successful for the range $\sim 800 \leqslant Re \leqslant \sim 5000$. This is a regime where each one of the film main elements—roll waves, ripples, capillary waves and substrate—can be effectively used to adjust a different statistical characteristic of the film. The geometrical profile of all types of waves is simulated fairly well by a log-normal function with its parameters related to specific wave features. The Gaussian fashion of selecting the wave parameters from specific ranges of values and the subsequent random deposition of the produced waves over the film substrate attests the stochastic nature of falling films. The performance of the code routine is satisfactory producing considerably good reconstructions of the film surface shape for all the data sets used to assess its accuracy. The potential for appraising several obscure features of falling films by matching the experimental and theoretical results is discussed.

Keywords: Falling film; Surface shape reconstruction; Modeling; Waves; Wave simulation

1. Introduction

Free falling films constitute an interesting field for both theoretical and experimental investigations with produced results of widespread utilization. They are usually encountered in common process equipment where heat and mass transfer take place (e.g. Collier, 1972). Regarding the

* Corresponding author. Tel.: +30-2310-99-7772; fax: +30-2310-99-7759.
E-mail address: karapant@chem.auth.gr (T.D. Karapantsios).

0301-9322/$ - see front matter © 2004 Elsevier Ltd. All rights reserved.
doi:10.1016/j.ijmultiphaseflow.2004.01.002

food industry, special attention has been directed towards the design and operation of direct contact falling film evaporators and condensers (e.g. Karapantsios et al., 1995). A significant amount of research work carried out over the last few decades, proves that the performance of such equipment is greatly influenced by the film characteristics and especially its surface waviness (e.g. Brauner and Maron, 1982; Webb, 1994). The enhancement of heat and mass transfer due to surface waves justifies the never lasting interest towards modeling of wavy falling films.

Numerous theoretical attempts have been made to study the waves formed on free falling liquid films. This wealth of research work can be somewhat arbitrarily divided in two general groups with respect to Reynolds number. The first group refers to wave evolution over laminar films flowing at low Reynolds numbers and it involves a number of different approaches. A considerable theoretical understanding was gained by the dynamic singularity analysis performed by Chang and co-workers (e.g. Chang et al., 1993; Chang, 1994; Chang and Demekhin, 2002), which derived close-form multiple solutions for the nonlinear evolution of finite amplitude waves bifurcating from primary perturbations on the smooth film. A few studies used finite element solutions of the full Navier–Stokes equations (e.g. Bach and Villadsen, 1984; Kheshgi and Scriven, 1987; Salamon et al., 1994) assuming waves with a finite amplitude or a stationary profile. Other efforts were based on simplified solutions of the Navier–Stokes equations under various approximations (e.g. permanent or periodic waves) or order-of-magnitude assumptions (e.g. Benney, 1966; Alekseenko et al., 1985; Nguyen and Balakotaiah, 2000). On the whole, the aforementioned analyses were found to produce waveforms that are only in fair agreement with experimental observations and only for small *Re* numbers—usually below 300—which are much lower than those usually encountered in many practical applications.

The second group of theoretical studies deals with films at higher *Re* numbers, where fast-moving large waves tend to overtake the small (capillary) waves resulting in a complicated wave structure. Numerical simulations of laminar wavy films at relatively high Reynolds numbers were conducted by a few investigators e.g. Wasden and Dukler (1989), Yu et al. (1995) and Stuhltrager et al. (1995), to predict the spatial variations in film thickness along with the velocity field inside solitary or interacting waves. Using a prescribed geometrical shape for large waves, Maron et al. (1985), Brauner (1987) and Maron et al. (1989) proposed a model which could yield some useful information regarding the velocity distribution within large waves, including also the effect of turbulence. Yet, the model was rather complex with different physical mechanisms controlling various zones along a large wave. Moreover, the employed shape of large waves—assumed to have a linear slope at both the front and the back of the waves—was oversimplified compared to that measured.

There is enough theoretical and experimental evidence that a falling film flow is transient and nonlinearly unstable and has a random character, especially at high Reynolds numbers where vortex motions prevail. Within the framework of deterministic chaos, some studies calculated the fractal dimensions of the reconstructed phase space from experimental film thickness measurements and verified that the nature of a falling film is indeed chaotic (e.g. Lacy et al., 1991; Drahos et al., 1997; Zhang et al., 2000). Accounting for such randomness, Back and McCready (1988) computed the local velocity gradients at the film surface (from reconstructions of the surface shape) by taking the inverse Fourier transform of the experimental wave amplitude spectra. In line with the above, Karapantsios and Karabelas (1990) determined a characteristic spatial evolution portrait of large waves independent of Reynolds number and used the computed Eulerian

surface accelerations to investigate the development of waves. Wave slopes in the range 14–20° for the wave front and −7° to −11.5° for the wave back were calculated, showing almost no dependence on Reynolds number.

Despite the significant amount of research work—both theoretical and experimental—carried out on free falling film characteristics, it is felt that additional effort is required to describe the wave surface geometrical details. This is more so if one considers that three-dimensional wave structures may flow even over laminar falling films (e.g. Adomeit and Renz, 2000). Recent works (e.g. Karimi and Kawaji, 1998; Takamasa and Kobayashi, 2000; Vlachogiannis and Bontozoglou, 2001; Mouza et al., 2002; Ambrosini et al., 2002) clearly indicate an evergreen interest for this research topic, where also the use of very sophisticated measuring techniques is highlighted.

This work is concerned with the reliable description of the surface morphology of wavy free falling films. The detailed experimental data obtained by Karapantsios et al. (1989) for thin falling films of water inside a 50 mm i.d. vertical pipe are employed to assess the proposed modeling procedure. In that work, parallel-wire electrical conductance probes were used for measuring instantaneous film thickness 2.5 m downstream from the water inlet. Data were collected over an 8 s period with a 500 Hz sampling frequency. A rather broad range of *Re* numbers was originally covered i.e. $509 \leqslant Re \leqslant 13{,}090$ but in the present study only data with Reynolds number below 7842 are tested. It should be stressed that the parallel-wire conductance probe method is considered a quite sensitive and accurate measuring technique in which the present authors have a considerable experience since they successfully employed it for measuring film thickness not only in free falling films (e.g. Karapantsios et al., 1989; Karapantsios and Karabelas, 1995a,b) but also in two-phase flow experiments (e.g. Vlachos et al., 1997). Although one-point film thickness measurements can not provide information about any 3D wave structures over a falling film, it is believed that principles and approximations advanced here regarding 2D waves may be extended to 3D waves as well.

In the following, the computational procedure is outlined first, and the method validation together with the main results are presented and discussed next.

2. Computational procedure

2.1. Preliminary analysis

2.1.1. Identification of large waves

It is commonly accepted that a falling liquid film is comprised mainly of (e.g. Chu and Dukler, 1975): (a) the *substrate*, a region of small thickness which at the one side is in contact with the solid wall while at the other side serves as the base to sustain the surface waves, (b) the *large waves* (also known as *roll waves*), which are waves with amplitude higher than the mean film thickness and which carry a significant portion of the total liquid flow, and (c) the *ripples*, which are waves with amplitude lower than the mean film thickness, covering the substrate between the large waves. The front of the large waves emerges from the substrate and has a steep slope while their back has a smaller slope and extends down to the substrate. Karapantsios et al. (1989) reported spectral density functions of film thickness for all the employed Reynolds numbers and found that they all displayed a very pronounced total maximum in the frequency range of 5–8 Hz which was

attributed to large waves. Modal frequencies of the same order were communicated also by other researchers (e.g. Chu and Dukler, 1975; Takahama and Kato, 1980; Zabaras, 1985). The major part of this study deals with experiments at $Re > 1000$ (i.e. for turbulent flow), where large amplitude waves cover the major part of the film surface (Karapantsios and Karabelas, 1990). Therefore, the first step of the present simulation is to identify and isolate these large waves.

The procedure of tracing the large waves in an experimental record, (thickness vs. time), initiates every time from the largest wave and continues in a descending order to the immediately smaller waves. The procedure ends when the total number of the recognized large waves represents a frequency of 5–8 Hz in the total duration of the sample (i.e. for a 8 s sample this means 40–64 waves). The identified waves can be either individual waves or part of formations of two or even three waves overlapping each other (Fig. 1a and b). In fact, this initial selection of large waves is made closer to 7–8 Hz because a small number of them will be rejected below as extreme outliers since their morphology is far too irregular.

2.1.2. Mathematical representation of large waves

The next step is to find an analytical expression that accurately depicts the geometrical profile of large waves. Simple polynomial functions are not acceptable since no distinct physical signif-

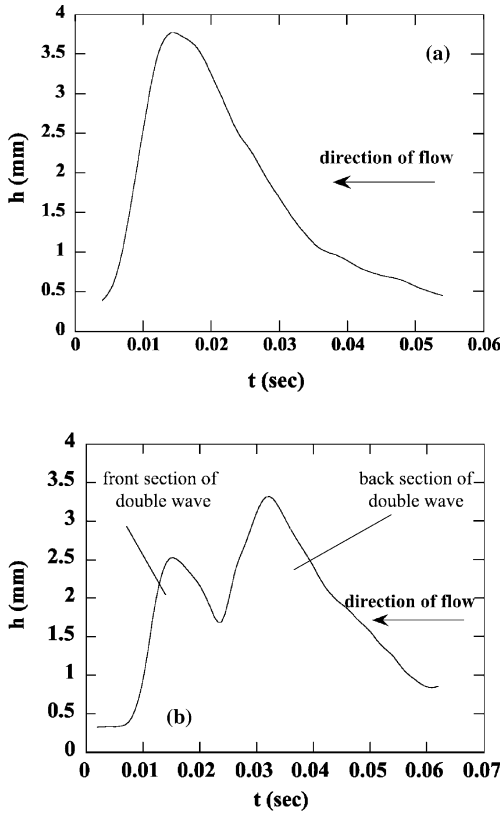

Fig. 1. (a) Individual large wave and (b) double wave, isolated from a measured film thickness record.

icance can be attached to their arithmetic coefficients regarding their role in shaping the theoretical curve. On the basis that most part of the flowing liquid is carried by large waves, the shape of the cumulative probability density function of the entire film thickness records can be attributed mainly to large waves. In this sense, it is reasonable to consider that the mathematical expressions describing the cumulative probability density functions of the whole sample can also describe satisfactorily the geometry of large waves. Karapantsios et al. (1989) reported that the cumulative probability density function of film thickness records in the range $509 \leqslant Re \leqslant 9000$ is best represented by a Weibull distribution, while a log-normal distribution is preferred at $9000 \leqslant Re \leqslant 13{,}090$. Takahama and Kato (1980) used a gamma distribution at $Re \leqslant 2400$, a log-normal at $2400 \leqslant Re \leqslant 4000$ and again a gamma distribution at $4000 \leqslant Re \leqslant 8000$. Telles and Dukler (1970) reported a satisfactory fit of their data with a gamma distribution in the range $1150 \leqslant Re \leqslant 5750$. The mathematical expressions for the Weibull, log-normal and gamma distributions can be found in any elementary statistical textbook, e.g. Derman et al. (1973).

Fig. 2 demonstrates that the above distributions are indeed quite successful in describing the profile of a typical large wave and that their predictions are in close proximity to each other. Among them, however, the log-normal distribution is more favorable to be employed in the present simulations since a quite distinct relationship was found to hold between its (four) parameters with specific physical characteristics of the examined waves, (see below). The log-normal distribution in its most generic form is given as follows (Derman et al., 1973):

$$y = \mathbf{a} + \mathbf{b} * \exp\left(-\frac{\ln \frac{x}{\mathbf{c}}}{2\mathbf{d}} \right)^2 \tag{1}$$

In this case, y stands for film thickness and x for time.

2.1.3. Parametric analysis of the log-normal distribution

Each parameter of the log-normal distribution (i.e. **a**, **b**, **c** and **d**) is found to be related to a certain physical feature of the geometry of the waves. More specifically, the parameter **a** corresponds to the minimum film thickness, $h_{\min}$, which is the thickness of the continuous substrate below the waves and in contact with the pipe inner walls. According to the data of Karapantsios

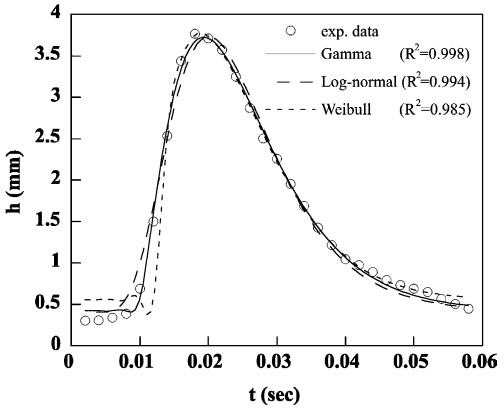

Fig. 2. Comparison of theoretical distribution curves with an experimental thickness trace of a large wave.

et al. (1989) for $Re <\sim 5000$, **a** is always around 0.25 mm. The parameter **b** dictates the amplitude of the theoretical log-normal curve. Fig. 3a presents the effect of **b** in the shape of the log-normal curve. A realistic range of **b**-values for the large waves isolated above, is $1 < \mathbf{b} < 4$. It is noted that the parameters **a** and **b** have both length dimensions, with the maximum (peak) value of the wave thickness given by $h_{\max} = \mathbf{a} + \mathbf{b}$.

Parameter **c** defines the relative position within each wave where the curve's maximum is located. In this work, this parameter takes values in the range $0.011 < \mathbf{c} < 0.022$ and has time

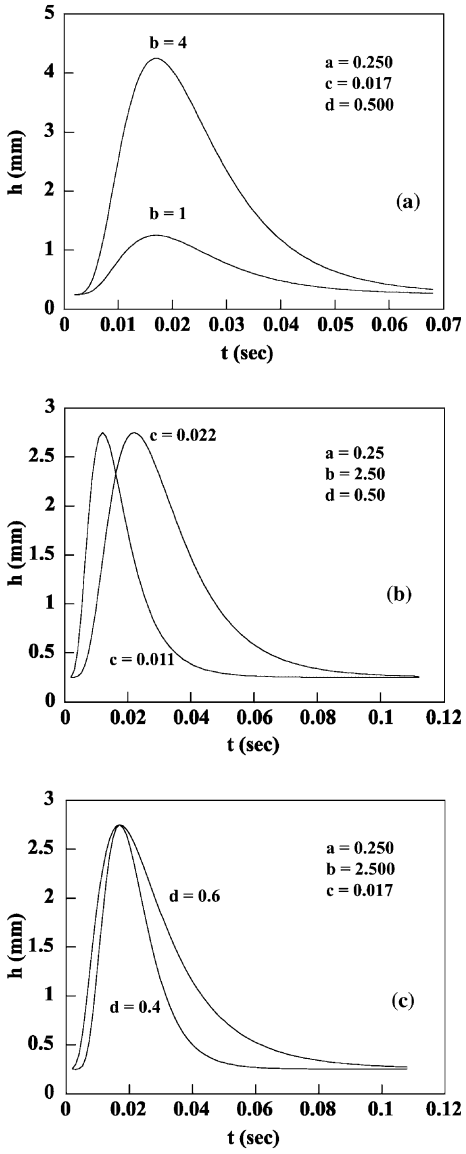

Fig. 3. Effect of (a) parameter **b**, (b) parameter **c** and (c) parameter **d**, on the shape of the log-normal curve.

dimensions since x in Eq. (1) denotes time. On the other hand, the dimensionless parameter **d** represents the wavelength (in fact, the time-length of the wave) and varies between $0.4 < \mathbf{d} < 0.6$. Fig. 3b and c shows the effect of **c** and **d**, respectively. It must be mentioned here that the notion of a "wavelength" is not exact when working with the log-normal curve. This is so because the log-normal curve tends asymptotically at large times to the horizontal line $y = \mathbf{a}$ (which expresses the substrate) and therefore the wavelength is, rigorously speaking, infinite. So, the term wavelength is used here only conventionally and reflects the time the curve takes to approach the horizontal asymptote $y = \mathbf{a}$ to 1% the value of **a**.

2.1.4. Dependence of the log-normal parameters on the Reynolds number

Fitting the log-normal function to every single one of the isolated large waves yields useful information regarding the variation of the log-normal parameters with Reynolds number and the possible interaction among them. The fitting of an individual large wave by the log-normal function is considered successful only when the correlation coefficient R^2 is above 0.9. The use of such a criterion is imperative because of the stochastic nature of film thickness, which sometimes leads to exceptionally irregular wave formations. It is worth mentioning, though, that R^2 was rarely below 0.93–0.95 for the identified waves of this work and rejection of waves based on this procedure is at most 5% of the initial selection. This leaves us with large waves still above 5 Hz.

Simple statistical analysis (ANOVA) reveals that for all the *Re* numbers examined here the interaction among the parameters **a**, **b**, **c** and **d** is not significant at a 95% level. Parameter **a** corresponds (as already mentioned) to the substrate height, $h_{\min}$, for which, after performing a linear regression analysis on the experimental data of Karapantsios et al. (1989), one obtains:

$$\mathbf{a} = h_{\min} = \begin{cases} 0.25 & \text{for } Re \leqslant 5500 \\ 0.0004Re + 0.0275 & \text{for } Re > 5500 \end{cases} \tag{2}$$

Fig. 4 presents the variation of the maxima and minima of the parameters **b**, **c** and **d** with respect to Reynolds number. For reasons that will be explained later the values $\mathbf{b}_{5\%}$ and $\mathbf{b}_{95\%}$ are used instead of the absolute values $\mathbf{b}_{\min}$ and $\mathbf{b}_{\max}$. Apparently, there is a clear linear dependence of parameter **b** on *Re* number while the parameters **c** and **d** are rather insensitive to *Re*. These observations are in accordance with Karapantsios et al. (1989) experimental findings, who reported that $h_{\max}$ increases linearly with *Re* whereas wave frequencies ($\propto 1/\mathbf{d}$) are independent from *Re*. The average best-fit **d** value, (0.50, computed from all *Re* numbers) corresponds to 23 data points in the film signal, which is the number of data points spanning the average large wave of this study. These 23 points represent an average large wave time-length of 0.046 s ($=23$ data points $*$ (500 data points/s)$^{-1}$). This value is a bit higher than 0.03 s which was proposed by Karapantsios et al. (1989) for the identification of large waves but much lower—as expected—than the values indicated by Fourier analysis (5–8 Hz $\rightarrow$ 0.2–0.125 s) which refer to the case of large waves covering completely the film surface with no space separating them.

It must be added here that the employed large wave-selection procedure (based on the one-by-one identification of progressively smaller waves until the 5–8 Hz frequency criterion is met) identifies large wave peaks always *well* above the mean film thickness, h_{mean}. In particular, it is found that the lowest wave peak height lies in the range:

$$\mathbf{a} + \mathbf{b}_{5\%} = (1.4\text{–}2.2) * h_{\text{mean}} \tag{3a}$$

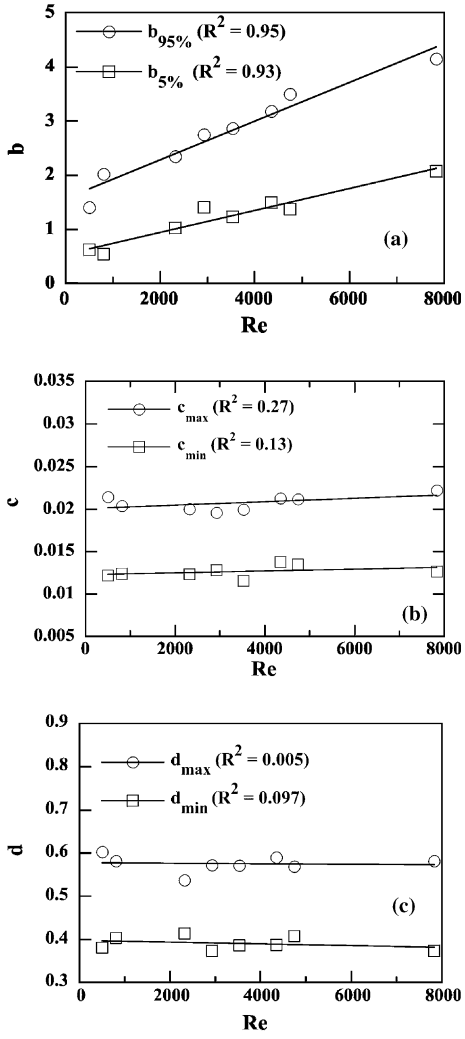

Fig. 4. Dependence of (a) parameter **b**, (b) parameter **c** and (c) parameter **d** on Reynolds number.

with no clear dependence on Reynolds number. In other words, the present analysis has selected no large wave peak in the spatial domain $[h_{\text{mean}}, (1.4\text{–}2.2) * h_{\text{mean}}]$ and the consequence of this will be discussed later. The situation improves only a little if one uses $\mathbf{b_{min}}$ instead of $\mathbf{b_{5\%}}$:

$$\mathbf{a} + \mathbf{b_{min}} = (1.2\text{–}2.0) * h_{\text{mean}} \tag{3b}$$

Table 1 summarizes the range of values of all the log-normal parameters estimated in the present analysis.

2.2. Algorithm development

It must be stressed already at this point that the success of the present algorithm in describing film thickness data constitutes a "sufficient" but not "necessary" term, regarding the undertaken

Table 1
Range of values of the log-normal parameters for the data of Karapantsios et al. (1989)

Parameter	Maximum	Minimum
a	0.25	for $Re \lesssim 5500$
	$0.0004Re + 0.0275$	for $Re > 5500$
b	$\mathbf{b}_{95\%} = 0.0003Re + 1.767$	$\mathbf{b}_{5\%} = 0.0002Re + 0.543$
$\mathbf{c}_{max}$	0.022	0.019
$\mathbf{c}_{min}$	0.014	0.011
$\mathbf{d}_{max}$	0.600	0.540
$\mathbf{d}_{min}$	0.410	0.370

assumptions and conventions. That is, there may be also other combinations of physical characteristics that can lead to equally well or even better simulation of the experimental data. The present algorithm claims only to be an adequate and reasonable on physical grounds choice for the description of the film surface geometry. Furthermore, the stepwise procedure of building-up the film morphology allowed us to attach specific significance to certain hydrodynamic features of the film and appreciate their interrelationships in the resulting film morphology.

The whole procedure aims at the successful step-by-step reconstruction of the main elements of the film thickness trace. In an ascending-height order, these are the substrate, the small amplitude waves or ripples and the large or roll waves. Computer implementation constraints dictated this order to be more or less the order of reconstruction. To start the procedure, the algorithm requires as inputs the *Re* number, the total duration of the simulation and the time interval, Δt, by which the time domain is discretized (time interval between successive data points). The values of the last two inputs are fixed for all the runs tested here, 8 and 0.002 s respectively, which are those employed by Karapantsios et al. (1989). To illustrate the computational procedure, a case for $Re = 2325$ is presented in detail below, where only 1 s of the simulated film trace is displayed for clarity.

2.2.1. Substrate reconstruction

This is a simple step consisting of the generation of a matrix with all its elements equal to the substrate height, $\mathbf{a} = h_{min}$ (Fig. 5a). All subsequent types of waves will be deposited over this substrate, therefore, for all waves $\mathbf{a} = h_{min}$.

2.2.2. Ripples reconstruction

Ripples are waves which have all their parts below the mean film thickness, h_{mean}, so they are distinctly smaller than roll waves. Yet, they appear to have an asymmetric profile similar to that of roll waves. So, the log-normal function may be employed for ripples reconstruction as well. Since the conductance technique of Karapantsios et al. (1989) did not permit the accurate spatial depiction of such small waves (the same holds also for Chu and Dukler, 1974), any information regarding ripples must be viewed with reservation. In view of the above, it is decided to perform the simulation of ripples assuming a geometric similarity with large waves. That is, parameters **c** and **d** are taken to lie between the limiting values identified for the large waves (Table 1). As

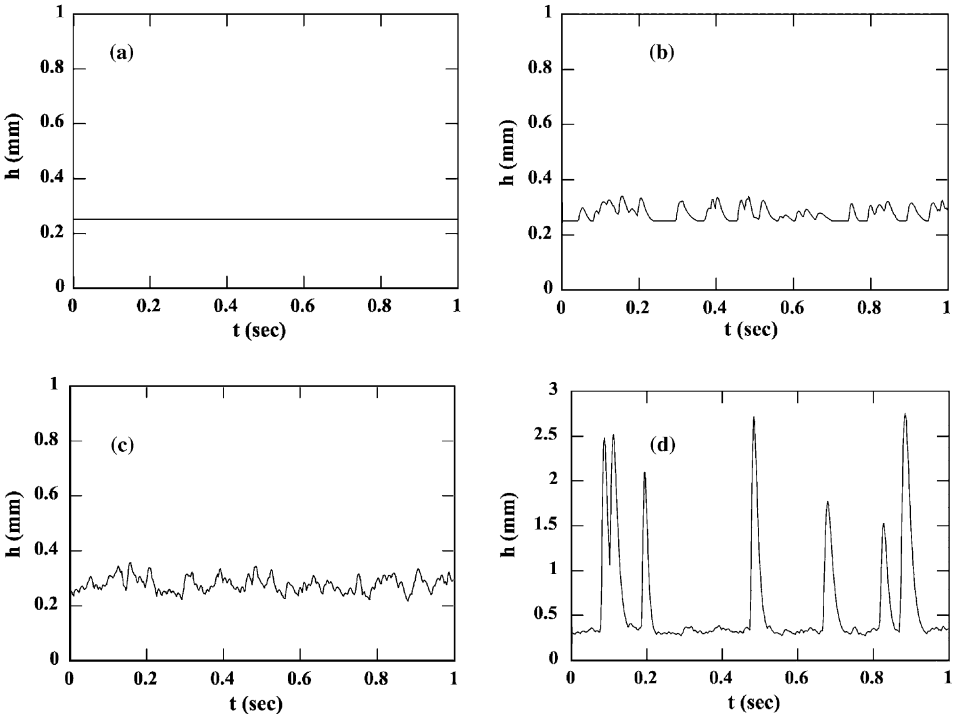

Fig. 5. (a) Simulation of the undisturbed substrate surface, (b) simulation of the substrate covered with ripples, (c) simulation of the substrate covered with both ripples and capillary waves (d) simulation of film thickness trace with capillary, ripples and large waves. All traces are for $Re = 2325$.

regards the value of **b**, this need not be rigorously predefined since the code has the ability to automatically adjust its value to meet the statistical criteria set for the film.

The frequency and location of occurrence of ripples on the surface of the film is a serious matter of concern. Karapantsios et al. (1989) argued about a frequency range between 10 and 20 Hz in their data while Chu and Dukler (1974) reported values about twice as high but they all agree that the range is rather independent from Reynolds number. However, the major difficulty in achieving an effective computer implementation comes from the fact that the ripples are encountered—and therefore must be deposited—in between large waves. This alternating wave deposition (i.e. large wave—small wave(s)—large wave) made the code exceedingly cumbersome and slow and therefore another approach was eventually employed.

The simulation of ripples starts by defining the frequency of waves that will be deposited on the substrate. This number is obtained from the empirical formula:

$$f = 0.011Re + 5 \tag{4}$$

The above expression was derived after extensive trials of the algorithm and comparisons of the simulated film thickness traces to experimental data. At first glance it looks improper that the frequency in Eq. (4) depends on Reynolds number. However, this is purely to counterbalance the increasing overlapping of ripples employed by the numerical scheme at higher Reynolds numbers. The code deposits first the ripples and then the large waves on the surface of the substrate. As the

Reynolds number increases, the deposited large waves have a much broader base (time-length) and so they overlap at a higher extent the pre-deposited ripples on the substrate, leaving in the end a comparable number of ripples for all *Re* numbers. The use of Eq. (4) is further supported by the fact that not only the frequency of occurrence of the ripples but also all other calculated statistics as well as the macroscopic appearance of the simulated film compare favorably well with the original experimental information. It should be emphasized that the relative comparisons were made not just for the ripples but for the entire reconstructed film including all kinds of waves.

The parameters **c** and **d** for all ripples are chosen in a random (Gaussian) manner from the domains $[\min \mathbf{c}_{\min}, \max \mathbf{c}_{\max}]$ and $[\min \mathbf{d}_{\min}, \max \mathbf{d}_{\max}]$, respectively. On the other hand, the parameter **b** receives initially random values from the arbitrary range $\mathbf{b}^{\mathrm{rpl}}_{\min} = 0.02$ to $\mathbf{b}^{\mathrm{rpl}}_{\max} = 0.1$. The choice of this range has no practical significance because the initially selected **b**-values for the ripples are adjusted later on by the code while performing correction tests. Next, each generated ripple is deposited in a Gaussian fashion over the undisturbed substrate surface. If parts of one ripple coincide with parts of another ripple that was previously deposited, then overlapping to greater heights occurs, that is, the parts with greater height are kept while the lower ones are rejected. At the end, overlapping yields a frequency smaller than the one estimated from Eq. (4) plus that the physical appearance of the surface is now more realistic because of the random occurrence of double, triple or even multiple ripples (Fig. 5b).

2.2.3. Capillary waves reconstruction

The substrate surface is not as smooth as one might have intuitively expected. Careful inspection of the experimental signals reveals that the substrate is covered by excessively dense disturbances of very low amplitude. Similar disturbances are also encountered at the surface of ripples but not on large waves. These small disturbances are capillary waves and represent a salient feature of a falling film's surface. Capillary waves originate from occasional hydrodynamic instabilities and/or the shearing action of the surrounding air and due to their small curvature, interfacial tension (capillary) forces have a restoring influence on them (e.g. Chu and Dukler, 1974). So, their reconstruction beyond the apparent esthetic reasons has also a physical significance.

The highly transient nature of capillary waves combined with the fact that the conductance probe of Karapantsios et al. (1989) could not resolve features down to the size of capillary waves, resulted in a rather chaotic appearance of capillary waves over the recorded film surface. In addition, the main statistical characteristics of the liquid film is practically unaffected by these small waves. For these reasons, it is decided to perform the reconstruction of capillary waves on a purely empirical basis.

For simplicity, a geometrical resemblance between ripples and capillary waves is assumed which means that the latter can be also represented by the log-normal function. However, this is not a crucial assumption as will be shown below. The selection procedure of the log-normal parameters **b**, **c** and **d** is the same as for the ripples but now the initial **b**-values are no further adjusted by the code. Regarding the frequency of deposition of capillary waves this has been empirically determined as *tenfold* the value obtained from Eq. (4) for the ripples.

The deposition procedure starts once more with the evaluation of the total number of capillary waves and their descriptive log-normal parameters, exactly as it was done with the ripples. Then, these waves are added in a Gaussian manner over the substrate and the ripples. In case a capillary

wave is deposited at a position where another wave already exists, then the higher parts of this wave replace those parts of the other wave with smaller height. Due to the exceedingly high number of deposited capillary waves, multiple overlapping occurs and as a result the finally reconstructed capillary waves end up loosing their original log-normal features. The result is illustrated in Fig. 5c. The above procedure is accepted on the basis that the macroscopic appearance of the final reconstructed film matches visually the morphology of the experimental signal. It must be kept in perspective that the frequency of ripples and capillary waves at this stage of the computations is different than at the final film due to the subsequent deposition of large waves.

2.2.4. Large waves reconstruction

With respect to large waves, the reconstruction procedure has much in common with the generation of ripples. The log-normal parameters **b**, **c** and **d** obtain their values randomly from the respective ranges in Table 1. The parameter **b** ranges between $\mathbf{b}_{5\%}$ and $\mathbf{b}_{95\%}$ and not between $\mathbf{b}_{min}$ and $\mathbf{b}_{max}$. This is done so because it is noticed that if the selection is made from the latter rigorous limit range then the whole simulation performs poorly, producing more wave peaks close to $\mathbf{b}_{min}$ and $\mathbf{b}_{max}$ than actually observed in the experiments. Possibly, the Gaussian manner of selecting **b** values for each large wave does not reflect exactly what happens in reality. The problem is surmounted by narrowing the range of parameter **b** between the statistical limits $\mathbf{b}_{5\%}$ and $\mathbf{b}_{95\%}$. The above clearly indicates that the simulation is particularly sensitive to the selection of the proper **b** values for the large waves, whereas it appears less dependent on the **c** and **d** values.

The frequency of occurrence of large waves is between 5 and 8 Hz (a value chosen randomly every time) according to which the algorithm produces the anticipated number of large waves. Prior to placing the large waves on the film surface, the hydrodynamic criterion reported by Karapantsios and Karabelas (1990), regarding the ratio of the front (max) to the back (min) slope of each wave, is checked if it applies:

$$1.5 < \left| \frac{(\mathrm{d}h/\mathrm{d}t)_{\max}}{(\mathrm{d}h/\mathrm{d}t)_{\min}} \right| < 3.0 \quad \text{for } Re \leqslant 5000 \tag{5a}$$

$$1.5 < \left| \frac{(\mathrm{d}h/\mathrm{d}t)_{\max}}{(\mathrm{d}h/\mathrm{d}t)_{\min}} \right| < 4.0 \quad \text{for } Re > 5000 \tag{5b}$$

In case the above condition is not met for some waves, the parameters **c** and **d** for these particular waves are re-selected, since the combination of **c** and **d** alone dictates the slopes of the log-normal waves. Following, all the large waves are deposited in a Gaussian manner over the film surface produced at the previous phase of the reconstruction (Fig. 5c). If parts of the large waves overlap with other elements of the film (such as capillary waves, ripples or other large waves) then the parts with the higher height remain. It must be noted that the large waves deposition does not have any significant effect on the frequency of large waves because it is very improbable a large wave to cover completely another large wave. On the contrary, the ultimate frequencies of capillary waves and ripples are drastically reduced. With the large waves in place, the reconstruction of the liquid film surface is complete and has the form shown in Fig. 5d.

In order for the simulation to be considered successful and terminate, the statistical characteristics of the reconstructed film thickness trace should match those obtained experimentally, for

the same *Re* number. On this account, the algorithm incorporates iterative control checks and adjustments until the desired result is achieved.

2.3. Checks and corrections

2.3.1. Standard deviation correction

As soon as the reconstruction of the whole film surface is completed for the first time, the standard deviation, σ, of the whole sample (8 s) is calculated. The obtained value is checked whether it is contained in between a specific range of values, which varies with Reynolds number. For $Re \leqslant 5500$ this range is

$$0.0001Re + 0.1132 < \sigma < 0.0001Re + 0.2046 \tag{6}$$

These limiting values are obtained from linear regression of the two independent sets of measurements reported by Karapantsios et al. (1989), for the range $509 \leqslant Re \leqslant 5500$. These authors have shown that for $Re > 5500$, the standard deviation is practically independent from *Re*, taking values in the range:

$$0.73 < \sigma < 0.79 \tag{7}$$

According to Karapantsios and Karabelas (1990), the change observed for $Re > 5500$ reflects the gradual weakening of the large waves amplification at these high flow rates. This was attributed to the progressive increase of the substrate thickness with respect to *Re*, Eq. (2), which accommodating now a larger portion of the flowing liquid acts as a dampener inhibiting the growth of roll waves.

As one might have expected, large waves appear to have a major impact on the value of the standard deviation of the whole film, since the latter expresses the dispersion of data around their mean value. The correction of the standard deviation of the simulated film is based on this observation. In particular, if the standard deviation falls outside the above ranges then the parameter **b** of a deposited large wave (picked in random), $\mathbf{b}_{\mathbf{old}}$, receives a new value, $\mathbf{b}_{\mathbf{new}}$, as follows. If σ is larger than the higher limits of Eq. (6) or (7) then $\mathbf{b}_{95\%}$ is replaced by $\mathbf{b}_{\mathbf{old}}$ and then $\mathbf{b}_{\mathbf{new}}$ is selected from the narrower range $[\mathbf{b}_{5\%}, \mathbf{b}_{\mathbf{old}}]$. On the other hand, if σ is smaller than the lower limits of Eq. (6) or (7) then $\mathbf{b}_{5\%}$ is replaced by $\mathbf{b}_{\mathbf{old}}$ and then $\mathbf{b}_{\mathbf{new}}$ is selected from the range $[\mathbf{b}_{\mathbf{old}}, \mathbf{b}_{95\%}]$. The just modified wave need not be checked for the hydrodynamic conditions of Eq. (5), since the parameter **b** has no effect on them.

The correction scheme described above, is repeated as many times as required (each time with a different randomly chosen wave), until the σ value falls inside the predefined range. This iterative procedure is rarely repeated for more than 6–10 waves of the total film (8 s). The simulated film thickness trace after the standard deviation correction is shown in Fig. 6. In the displayed time span of 1 s, only the (double) large wave on the left has been modified.

2.3.2. Mean value correction

It is imperative the mean value of the simulated film to also fall inside a specific range of values. The limits of this range are defined through a linear (for simplicity) regression of the two independent data sets of Karapantsios et al. (1989). Hence, it follows:

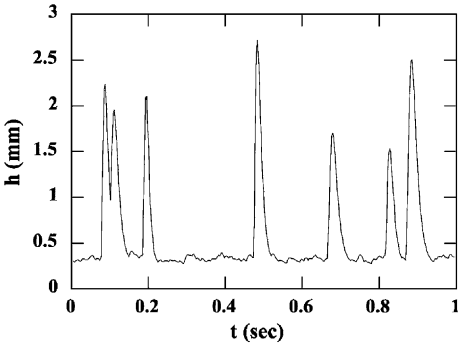

Fig. 6. Simulated film thickness trace for $Re = 2325$ after the standard deviation correction.

$$0.00009Re + 0.3949 < h_{\text{mean}} < 0.0001Re + 0.4247 \tag{8}$$

Eq. (8) is valid for the whole range of Re numbers tested, i.e. 509–7842. Instead of requiring h_{mean} of the reconstructed film to satisfy Eq. (8), a different procedure is followed. From the range denoted by Eq. (8), a target mean value, $\bar{h}$, is chosen in a Gaussian manner, against which the mean value of the simulation data is contrasted. This procedure is preferred because the algorithm spontaneously tends to produce mean values nearer to the lower limit of Eq. (8), instead of values uniformly distributed over the entire range.

In case where the mean value of the reconstructed film, h_{mean}, deviates from $\bar{h}$, a correction is made. The remedial action applies only to the substrate and to the ripples. The adjustment of solely these two film elements proved adequate in effectively approaching $\bar{h}$, without spoiling the preceding standard deviation correction applied to large waves, as confirmed by the successful simulation outcome. The computational convenience in using completely independent correction actions for the standard deviation and for the mean value is evident although on physical grounds a weighted contribution of all film elements to all statistical quantities would be more appropriate.

The correction procedure starts by comparing the simulation mean value, h_{mean}, to the target mean value, $\bar{h}$. If the two values differ from each other by more than $\pm 1\%$, the first action is to check whether shifting the substrate height—by adding or subtracting a small constant thickness to the entire simulated trace—brings h_{mean} close enough to $\bar{h}$. The reconstructed film is allowed to shift by no more than ± 0.01 mm. This is the maximum acceptable fluctuation of the substrate height, as determined from the data of Karapantsios et al. (1989). Next, the total minimum of the modified film trace is calculated which is actually the new height of the substrate, $\mathbf{a}'$. The value of $\mathbf{a}'$ must satisfy the double inequality

$$h_{\min} - 0.01 < \mathbf{a}' < h_{\min} + 0.01 \tag{9}$$

If the above substrate adjustment is not enough to correct the mean value of the simulated film, a correction of ripples is advanced. In order to achieve this, a whole new calculation starts from the beginning of Section 2.2, because adjusting one or more of the already created ripples is neither convenient nor effective. This is due to the extensive overlapping among ripples as a result of which it is not anymore easy to identify and implement changes to any of them. So, from a computational point of view it is better to simply adjust the range of the necessary parameters for the ripples and start all over again the reconstruction of the film. The information regarding the

previously selected large waves is also not retained in this new round of calculations. This is because it is often the case that with the new ripples, the standard deviation correction must be also repeated and once this is started the gain from keeping the old large waves virtually vanishes.

In this new set of calculations, all the parameters are selected again in a random fashion utilizing the aforementioned limiting ranges and correlations but the target mean value $\bar{h}$ is kept the same as before. The important differentiation in these new calculations is that the parameter **b** of the ripples does not receive random values from the range $[\mathbf{b}_{\mathbf{min}}^{\mathbf{rpl}}, \mathbf{b}_{\mathbf{max}}^{\mathbf{rpl}}]$, but instead from the range $[\mathbf{b}_{\mathbf{min}}, \mathbf{b}'_{\mathbf{max}}]$, where $\mathbf{b}'_{\mathbf{max}}$ is given by the following relation:

$$\mathbf{b}'_{\mathbf{max}} = \mathbf{b}_{\mathbf{max}} + \mathbf{a}' - h_{\min} \tag{10}$$

and $\mathbf{b}_{\mathbf{min}}$ and $\mathbf{b}_{\mathbf{max}}$ are, respectively, the lower and higher **b**-values attained by the ripples at the end of the previous round of calculations. It must be noted that $\mathbf{b}'_{\mathbf{max}}$ never reaches values above h_{mean} or $\bar{h}$. Apart from the mean value correction, the computational gain from the above manipulation of the ripples' **b**-values, regarding the time needed to achieve convergence, is substantial.

The reconstruction process, including the corrections for the standard deviation and the mean value, is iterated until the produced results fulfil the conditions set for these two statistical parameters. Fig. 7 shows the new film thickness trace produced at the end of the mean value correction. Comparing Figs. 6 and 7 it is evident that the two displayed traces are quite different in appearance due to the fact that the mean value correction procedure leads every time to a completely new film surface with large waves, ripples and capillary waves different than the previous ones. Yet, their frequency of occurrence plus all other statistical quantities are within the desired range (calculated for the entire sample, 8 s).

2.3.3. Cumulative probability density function correction

As observed by previous investigators (Chu and Dukler, 1974, 1975; Takahama and Kato, 1980; Karapantsios et al., 1989) the probability density distribution (PDD) of the measured film thickness signal is asymmetric with a long tail to the right. In such cases the mean value and standard deviation of the sample are not adequate descriptors of the distribution but statistical moments of higher order are required, e.g. the coefficients of skewness and kurtosis, to represent the shape of the PDD in terms of its deviation from the normal distribution. For this reason, the last check of the algorithm deals with adjusting the PDD of the reconstructed time series. This is

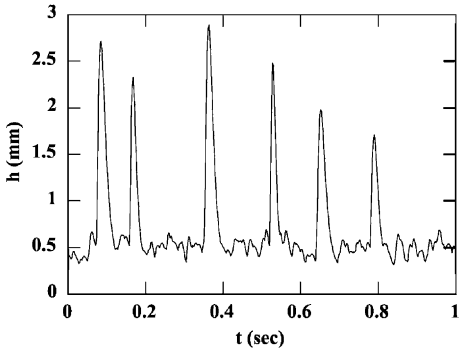

Fig. 7. Simulated film thickness trace for $Re = 2325$ after the mean value correction.

necessary because it is possible for a reconstructed sample to have the same mean value and standard deviation with an experimental sample but a quite different PDD. Karapantsios et al. (1989) reported a satisfactory fit of the cumulative probability density distributions (CPDD) of their film thickness records—for the range of *Re* numbers tested—by the Weibull distribution.

The Weibull probability density function is a special case of a Pearson type III or generalized Gamma distribution. If film thickness is represented in the form $h - h_{\min}$, then the distribution according to the Weibull probability density function becomes (Derman et al., 1973):

$$f(h) = \frac{k}{\gamma}\left(\frac{h - h_{\min}}{\gamma}\right)^{k-1} \exp\left(-\left(\frac{h - h_{\min}}{\gamma}\right)^{k}\right) \tag{11}$$

where k is the *shape* parameter and γ the *scale* parameter of the distribution. If h_{mean}, $h_{\min}$ and σ of the sample are known then the following equations can be used to find k and γ (Γ is the gamma function):

$$\left(\frac{\sigma}{h_{\text{mean}} - h_{\min}}\right)^2 = \frac{\Gamma(1 + 2/k)}{(\Gamma(1 + 1/k))^2} - 1 \tag{12a}$$

$$\gamma = \frac{h_{\text{mean}} - h_{\min}}{\Gamma(1 + 1/k)} \tag{12b}$$

Evidently, Eqs. (12a) and (12b) are cumbersome from a computational standpoint and for this reason, other convenient algebraic expressions are employed in their place in the present algorithm. An acceptable approximation ($\sim \pm 0.1\%$) derived for the values of k when the ratio $\sigma/(h_{\text{mean}} - h_{\min})$ varies between 0.7 and 1.2 (as is the case with the data of Karapantsios et al., 1989) is

$$k = \left(\frac{\sigma}{h_{\text{mean}} - h_{\min}}\right)^{-1.031} \tag{13a}$$

In the same range of $\sigma/(h_{\text{mean}} - h_{\min})$ values, γ can be approximated to within 1% by

$$\gamma = \frac{2 \cdot (h_{\text{mean}} - h_{\min})}{\sqrt{\pi}} \tag{13b}$$

For a wider $\sigma/(h_{\text{mean}} - h_{\min})$ interval or for accuracy better than 0.01%, γ can be represented by

$$\gamma = (h_{\text{mean}} - h_{\min}) \cdot \frac{k^{2.6674}}{0.184 + 0.816 \cdot k^{2.73855}} \tag{13c}$$

The correction procedure starts by calculating the parameters k and γ from Eqs. (13a) and (13c). Then, the entire simulated h series (as obtained after the mean value correction), is sorted in ascending order. Subsequently, the values of the CPDD are calculated for every film thickness position between $h_{\min}$ and $h_{\max}$. The resulting $f(h)$ values are used to solve the inverse Weibull function with h as the unknown.

The latter values (henceforth referred to as the Weibull predictions, h_{W}) are compared to the corresponding h values of the simulated series (Fig. 8a). In order to judge whether a correction is needed, the average of the percentage deviations between each element of the Weibull curve and the simulation curve is calculated. If this number is less or equal to the number predicted by

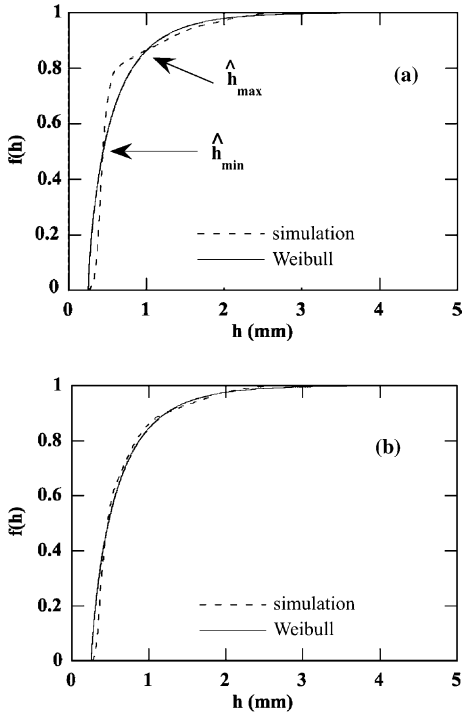

Fig. 8. Comparison of the theoretical Weibull CPDD vs. the corresponding curve from the simulation data (a) without any correction applied to the CPDD and (b) after the final correction of the CPDD. Results are for $Re = 2325$.

$$N = 4.4122 * \exp(0.0003Re) \tag{14}$$

then the program terminates. Eq. (14) has been determined empirically after extensive comparisons of the experimental data of Karapantsios et al. (1989) with best-fit Weibull distributions and represents the overall closest possible that the theoretical distribution approached the measurements, for all the employed Re numbers. In developing Eq. (14), points with cumulative probability values less than 0.1 are neglected since they correspond to very small heights not playing an important role to film morphology but for which the percentage deviations between curves can reach high values.

Initially, the shape of the two curves in Fig. 8a is quite different and the limitation posed by Eq. (14) is not met. Then, the points of interception of the two curves are determined. There are always two such points for all the examined Reynolds numbers. The first point, $f(\hat{h}_{\min})$, receives values from 0.4 (40% of the population) for $Re = 812$ to 0.6 (60% of the population) for $Re = 4745$, whereas the second point, $f(\hat{h}_{\max})$, remains approximately constant around 0.85 (85% of the population), regardless the Re.

As can be seen, above the higher interception point, $f(\hat{h}_{\max})$, there is a quite satisfactory convergence between the two curves. This part of the curves corresponds to film heights representing the upper half of the large waves. For $0.1 < f(h) < 0.4$ the two curves are again quite close to each other, this section representing chiefly the ripples. It must be recalled here that the height of the produced ripples never exceeds h_{mean} (which has a nearly constant probability value

$f(h_{\text{mean}}) = 0.65$–$0.7$). However, the simulated section between $\hat{h}_{\max}$ and $\hat{h}_{\min}$ deviates considerably from the theoretical curve and violates the condition of Eq. (14). After examination of many simulated curves, it is found that there exist no large wave or ripple with its peak in between the two interception points. Thus, this section of the curve represents solely the lower part of large waves. This is due to the employed wave-selection criteria which being different for the large waves and the ripples, do not yield wave peaks with intermediate **b**-values in the range $[\mathbf{b}'_{\mathbf{max}}, \mathbf{b}_{\mathbf{5}\%}]$. It is noteworthy though, that despite this irregularity both the mean value and the standard deviation of the reconstructed sample are within the desired ranges.

The deviation of the two curves in Fig. 8a is corrected via the random deposition of additional waves of intermediate size at the liquid film surface which, for simplicity, they are also assumed to have a log-normal shape. The number of the waves that are deposited on the film, every time the CPDD correction step is energized, is obtained empirically from the formula:

$$m = \frac{1}{3} * \frac{f(\hat{h}_{\max}) - f(\hat{h}_{\min})}{23} * \frac{T}{\Delta t} \tag{15}$$

where T and Δt are the total sample time and discretization interval (8 and 0.002 s, respectively), 23 is the number of data points of the average large wave of this study (see Section 2.1.4) and 1/3 is an empirical factor to improve the convergence characteristics of the algorithm. Eq. (15) in fact divides the number of data points between the two interception points by the average large wave time-length to determine how many of such average waves fit in this section and then reduces this value by a factor of three. If instead of m waves, just a single wave is added every time to the simulated trace then the convergence is excessively slow. On the other hand, if m in Eq. (15) is not divided by three then there are cases where the simulated curve already after the first addition of the intermediate waves deviates to the other side of the Weibull curve (overcorrection). For $Re = 2325$, it is $f(\hat{h}_{\min}) = 0.51$ and $f(\hat{h}_{\max}) = 0.87$ from which one obtains $m = \{1/3 * (f(\hat{h}_{\max}) - f(\hat{h}_{\min}))/23\} * 8/0.002 = 21$ which is the number of the intermediate waves deposited at the first corrective action of the CPPD. For any subsequent correction of the CPPD this number is reduced because the updated $f(\hat{h}_{\min})$ and $f(\hat{h}_{\max})$ values are much closer to each other. Usually, the required total number of deposited waves to satisfy the CPPD criterion does not exceed 30–35 (for 8 s total simulation period), regardless of Re. It must be stressed, however, that the real population of these intermediate waves on the film surface is a bit less because of overlapping by the already existing large waves.

After the number of the intermediate waves is determined, the log-normal parameters **b**, **c** and **d** of each wave are assigned their values. Regarding the parameters **c** and **d**, the same rules apply as with the ripples and large waves. On the other hand, the parameter **b** is selected randomly from the range $[\mathbf{b}^{\mathbf{int}}_{\mathbf{min}}, \mathbf{b}^{\mathbf{int}}_{\mathbf{max}}]$, where

$$\mathbf{b}^{\mathbf{int}}_{\mathbf{max}} = \hat{h}_{\min} - a \tag{16}$$

$$\mathbf{b}^{\mathbf{int}}_{\mathbf{max}} = \hat{h}_{\max} - a \tag{17}$$

Examinations for all the employed Re numbers showed that

$$\mathbf{b}'_{\mathbf{max}} < \mathbf{b}^{\mathbf{int}}_{\mathbf{min}} < \mathbf{b}^{\mathbf{int}}_{\mathbf{max}} < \boldsymbol{b}_{\mathbf{5}\%} \tag{18}$$

which means that indeed the new intermediate waves have peak values always in between the already reconstructed ripples and large waves. Fig. 8b contrasts the cumulative probability density curve after its final correction against the theoretical Weibull curve.

When the criterion of Eq. (14) is satisfied, the code stores the information about the total number of the deposited intermediate waves and the limits between which their parameter **b** receives its values. Following, the new reconstructed film surface undergoes a recheck for all of the aforementioned statistical quantities. If a new correction of the mean value is needed ($\bar{h}$ remains always the same) the procedure is as described above and after this is finished, intermediate waves are added to the film. These intermediate waves are not entirely new in the sense that they maintain their total number and b-values from the earlier round of the CPPD correction but their position on the surface of the film is reselected in a random manner. The execution sequence of the code routine is presented schematically in Fig. 9.

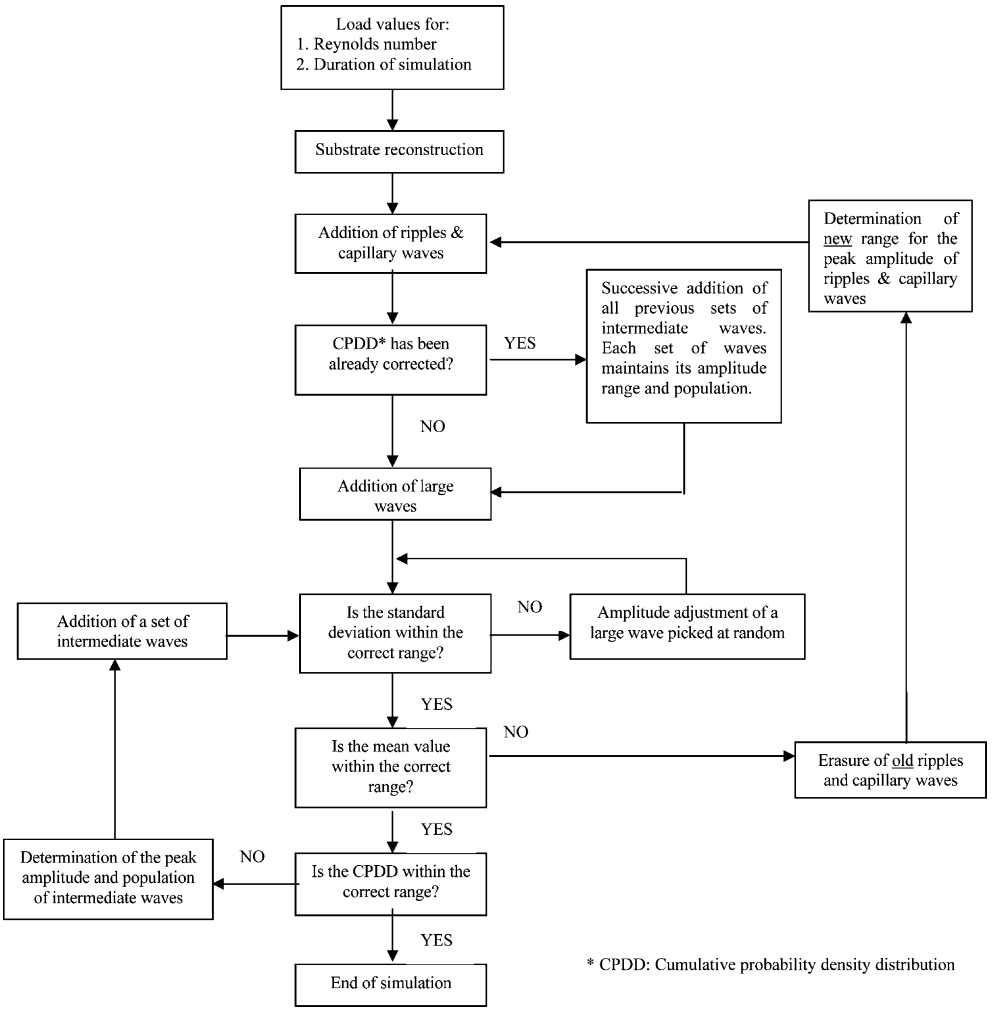

Fig. 9. Block diagram of code routine.

3. Results and discussion

The lowest and the highest Reynolds numbers for which the above algorithm proved effective is 812 and 4745, respectively. Outside this range the algorithm is not possible to converge. This is, however, an artifact resulting from the concept to correct the mean value of the simulated signal by exclusively adjusting the ripples (and the substrate) whereas the standard deviation of the signal by adjusting only the roll waves. Thus, for the examined $Re = 509$, the simulated roll waves are larger than in the real film and this is so because in this case (wavy laminar film) the size of the ripples is too small to can effectively control the mean value of the film; so the large waves influence decisively both the standard deviation and the mean value. On the other hand, for $Re = 5517$ and particularly for $Re = 6682$ and 7842, the distinction between ripples and roll waves is not so clear since now the ripples grow to considerable heights. So, the mean value correction has also a serious effect on standard deviation and vice versa. This is in line with the physical picture of the film presented by Karapantsios et al. (1989) and Karapantsios and Karabelas (1990), according to which for $Re > 5000$ the amplification of roll waves reduces drastically and instead the substrate starts to grow. Accordingly, Grossman (1984) considered the regime $1000 < Re < 4000$ not to be yet fully turbulent but a transitional inertial wavy-turbulent flow regime.

Fig. 10 shows a comparison between the liquid film height traces obtained experimentally vs. those produced by the simulation process for the successful range of Reynolds numbers. The plots are for $Re = 812$, 2325 and 4745. The one-point film thickness time records of Karapantsios et al. (1989) does not permit evaluation of the average roll wave velocity at each Re. Approximate values can be obtained by interpolation among the elements of a comparable data set reported by Karapantsios and Karabelas (1995a), obtained at the same longitudinal distance of the test pipe and within the same range of Reynolds numbers. These velocities are 1.23, 1.4 and 1.8 m/s, for $Re = 812$, 2325 and 4745, respectively. The simulation results are quite satisfactory, keeping in mind the stochastic nature of the film surface. Hence, the criteria employed for the reconstruction of the free falling film surface morphology can be considered as pretty effective.

An effort is made to determine the minimum duration of the simulation, for which reliable results can be obtained. This is the time required for the mean and the standard deviation values of the sample to stabilize. Fig. 11 shows a representative graph (for $Re = 2325$) of these two statistical quantities plotted against time. It can be safely argued that for a simulation duration of approximately 4 s both h_{mean} and σ attain almost constant values. What is perhaps more significant is that the respective experimental values require about the same time to level off. The discrepancy between the final experimental and simulated values is within the ranges defined by Eqs. (6) and (8).

Another interesting result refers to the spectra density functions of film height. According to Karapantsios et al. (1989), the modal frequency of the large waves is 5–8 Hz, while a second less pronounced peak appears at frequencies of 10–20 Hz corresponding to the smaller waves in the substrate. The above observations hold for the entire range of Reynolds numbers tested. Similar results are obtained from the simulation data, as displayed in Fig. 12. The absolute maximum of the spectra graphs corresponds to the characteristic frequency of large waves whereas the secondary peaks between 10 and 20 Hz are attributed mainly to the reconstructed intermediate waves.

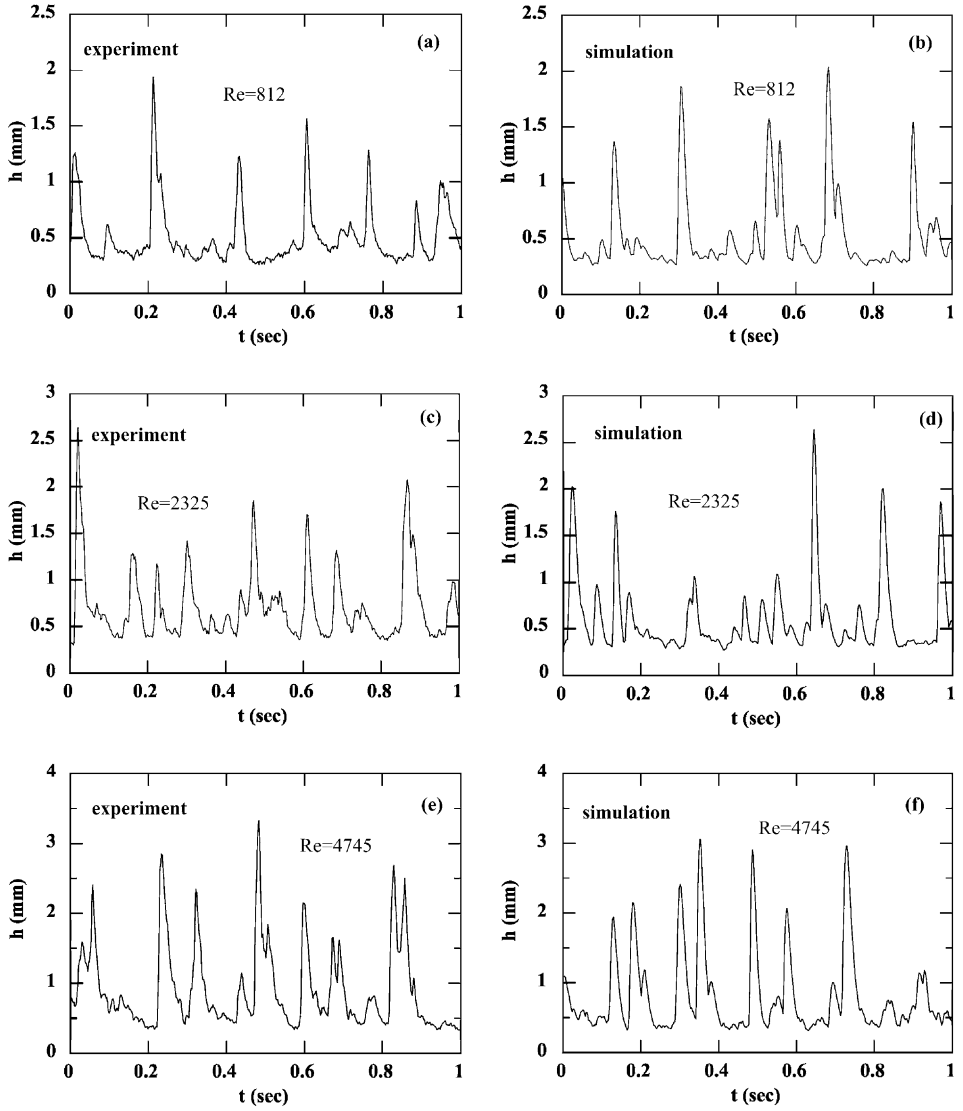

Fig. 10. Liquid film thickness traces for $Re = 812$, 2325 and 4745: (a), (c), (e) experiment and (b), (d), (f) simulation (for clarity, only 1 s is shown).

An important feature of this work is that the log-normal parameters **c** and **d** receive their values from the same range, for all wave categories. In fact, the only difference between the various types of waves refers to the parameter **b**, which is related to the wave height. Therefore, it can be assumed that all wave types are geometrically alike. Capillary waves can be excluded from this argument because of the extensive overlapping that occurs during their reconstruction so that they end up with a quite different, than the log-normal, shape. But even in the experimental signals, geometrical asymmetry is improbable for such small curvature waves due perhaps to the strong restoring influence of interfacial tension forces.

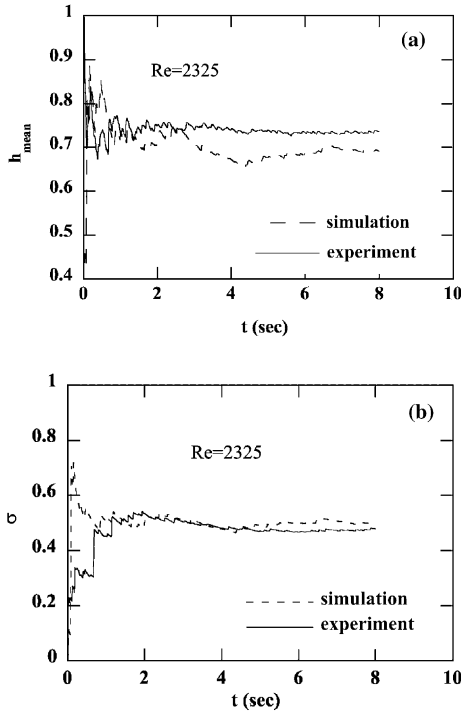

Fig. 11. (a) Mean value vs. time and (b) standard deviation vs. time, for simulated and experimental data ($Re = 2325$).

Finally, it is worth mentioning some characteristics of the intermediate type of waves that are produced during corrections of the CPDD. These waves have a size in between the sizes of large waves and ripples. If one considers the highly dynamic nature of a falling film, that does not permit wave structures to maintain their integrity for long downstream distances—the cross-correlation coefficient computed for simultaneous film thickness records sampled at stations apart by more than 40 cm is very low, e.g. Karapantsios and Karabelas, 1995a—then these intermediate waves might be viewed either as ripples that grow bigger or large waves that get smaller. In this respect, the number of the intermediate waves over a certain time period may reflect the rate of creation and destruction of large waves. Taking into account that the characteristic frequency of the large waves remains almost constant in every downstream longitudinal position (Takahama and Kato, 1980; Karapantsios and Karabelas, 1995a), it can be assumed that, on the average, the rate of large waves destruction is counterbalanced by the rate of their creation. Such an observation has a great significance because the rate of large waves renewal is very important in understanding the mechanisms of heat and mass transport across a falling film in terms of the wave-induced turbulence and the ensuing mixing of the liquid layers near the free surface.

4. Conclusions

In the present study a simulation algorithm is presented for the surface morphology reconstruction of free falling films at relatively high Re numbers, i.e. $\sim 800 < Re < \sim 5000$. Several

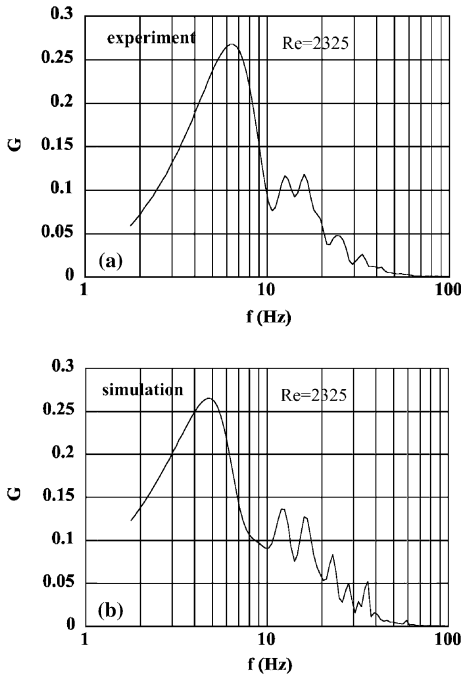

Fig. 12. Power spectra for $Re = 2325$: (a) experiment and (b) simulation.

types of waves have been considered to contribute differently in the development of the free surface. These are the roll waves, the ripples and the capillary waves. The geometrical profile of all these waves is assumed to be satisfactory described by the log-normal function. An important feature of the present analysis is that it is possible to tune the standard deviation of the reconstructed film by adjusting exclusively some of the roll waves (in random) while the mean value of the film by adjusting some of the ripples (and/or the substrate), accordingly. The performance of the simulation is encouraging, producing acceptable predictions. This demonstrates that the criteria and hypotheses incorporated in the algorithm are capable of simulating the surface morphology fairly accurately. However, the possibility must not be excluded that there may exist other combinations of physical characteristics that can also lead to acceptable predictions. Nonetheless, the solution presented here is a useful tool in modeling efforts. This work suggests that simulation efforts like the present one may facilitate the exposure of concealed salient features of the film flow, such as the rate of large waves renewal, which are essential to comprehend the impact of waves on processes where heat and mass transfer hold a key role.

Acknowledgements

Grateful acknowledgement is made of the financial support by the Research Committee of the Technological Educational Institution of Serres.

References

Adomeit, F., Renz, U., 2000. Hydrodynamics of three-dimensional waves in laminar falling films. Int. J. Multiphase Flow 26, 1183–1208.

Alekseenko, S.V., Nakoryakov, V.E., Pokusaev, B.G., 1985. Wave formation on vertical falling liquid films. Int. J. Multiphase Flow 11, 607–627.

Ambrosini, W., Forgione, N., Oriolo, F., 2002. Statistical characteristics of a water film falling down a flat plate at different inclinations and temperatures. Int. J. Multiphase Flow 28, 1521–1540.

Bach, P., Villadsen, J., 1984. Simulation of the vertical flow of a thin wavy film using a finite-element method. Int. J. Heat Mass Transfer 27, 815–827.

Back, D.D., McCready, M.J., 1988. Theoretical study of interfacial transport in gas–liquid flows. AIChE J. 34, 1789–1802.

Benney, D.J., 1966. Long waves on liquid films. J. Math. Phys. 45, 150–155.

Brauner, N., 1987. Roll wave celerity and average film thickness in turbulent wavy film flow. Chem. Eng. Sci. 42, 265–273.

Brauner, N., Maron, D.M., 1982. Characteristics of inclined thin films, waviness and the associated mass transfer. Int. J. Heat Mass Transfer 25, 99–110.

Chang, H.C., 1994. Wave evolution on a falling film. Ann. Rev. Fluid Mech. 26, 103–136.

Chang, H.C., Demekhin, E.A., 2002. Complex Wave Dynamics on Thin Films. Elsevier, Amsterdam.

Chang, H.C., Demekhin, E.A., Kopelevich, D.I., 1993. Nonlinear evolution of waves on a falling film. J. Fluid Mech. 250, 433–480.

Chu, K.J., Dukler, A.E., 1974. Statistical characteristics of thin, wavy films, Part II. Studies of the substrate and its wave structure. AIChE J. 20, 695–706.

Chu, K.J., Dukler, A.E., 1975. Statistical characteristics of thin, wavy films, Part III. Structure of the large waves and their resistance to gas flow. AIChE J. 21, 583–593.

Collier, J.G., 1972. Convective Boiling and Condensation. McGraw-Hill, London.

Derman, C., Gleser, L.J., Olkin, I., 1973. A Guide to Probability Theory and Applications. Holt, Rinehart & Winston, New York.

Drahos, J., Tihon, J., Sobolik, V., Hasal, P., Schreber, I., Marek, M., 1997. Analysis of wave modes in liquid film falling down a vertical oscillating plate. Chem. Eng. Sci. 52, 1163–1176.

Grossman, G., 1984. Heat and mass transfer in film absorption. In: Cheremisinoff, N.P. (Ed.), The Handbook for Heat and Mass Transfer Operations. Gulf.

Karapantsios, T.D., Karabelas, A.J., 1990. Surface characteristics of roll waves on free falling films. Int. J. Multiphase Flow 16, 835–852.

Karapantsios, T.D., Karabelas, A.J., 1995a. Longitudinal characteristics of wavy falling films. Int. J. Multiphase Flow 21, 119–127.

Karapantsios, T.D., Karabelas, A.J., 1995b. Direct-contact condensation in the presence of noncondensables over free-falling films with intermittent liquid feed. Int. J. Heat Mass Transfer 38, 795–805.

Karapantsios, T.D., Paras, S.V., Karabelas, A.J., 1989. Statistical characteristics of free falling films at high Reynolds numbers. Int. J. Multiphase Flow 15, 1–21.

Karapantsios, T.D., Kostoglou, M., Karabelas, A.J., 1995. Local condensation rates of steam–air mixtures in direct contact with a falling liquid film. Int. J. Heat Mass Transfer 38, 779–794.

Karimi, G., Kawaji, M., 1998. An experimental study of freely falling films in a vertical tube. Chem. Eng. Sci. 53, 3501–3512.

Kheshgi, H.S., Scriven, L.E., 1987. Distributed film flow on a vertical plate. Phys. Fluids 30, 990–997.

Lacy, C.E., Sheinsuch, M., Dukler, A.E., 1991. Methods of deterministic chaos applied to the flow of thin wavy films. AIChE J. 37, 481–489.

Maron, D.M., Brauner, N., Dukler, A., 1985. Interfacial structure of thin falling films: piecewise modelling of the waves. Physicochem. Hydrodyn. 6, 87–113.

Maron, D.M., Brauner, N., Hewitt, G.F., 1989. Flow patterns in wavy thin films: numerical simulation. Int. Commun. Heat Mass Transfer 16, 655–666.

Mouza, A.A., Paras, S.V., Karabelas, A.J., 2002. The influence of small tube diameter on falling film and flooding phenomena. Int. J. Multiphase Flow 28, 1311–1331.

Nguyen, L.T., Balakotaiah, V., 2000. Modeling and experimental studies of wave evolution on free falling liquid films. Phys. Fluids 12, 2236–2256.

Salamon, T.R., Armstrong, R.C., Brown, R.A., 1994. Travelling waves on inclined films: numerical analysis by the finite-element method. Phys. Fluids 6, 2202–2220.

Stuhltrager, E., Miyara, A., Uehara, H., 1995. Flow dynamics and heat transfer of a condensate film on a vertical wall—part II. Flow dynamics and heat transfer. Int. J. Heat Mass Transfer 38, 2715–2722.

Takahama, H., Kato, S., 1980. Longitudinal flow characteristics of vertically falling liquid films without concurrent gas flow. Int. J. Multiphase Flow 6, 203–215.

Takamasa, T., Kobayashi, K., 2000. Measuring interfacial waves on film flowing down tube inner wall using laser focus displacement meter. Int. J. Multiphase Flow 26, 1493–1507.

Telles, A.S., Dukler, A.E., 1970. Statistical characteristics of thin, vertical, wavy, liquid films. Ind. Eng. Chem. Fundam. 9, 412–421.

Vlachogiannis, M., Bontozoglou, V., 2001. Observations of solitary wave dynamics of film flows. J. Fluid Mech. 435, 191–215.

Vlachos, N.A., Paras, S.V., Karabelas, A.J., 1997. Liquid-to-wall shear stress distribution in stratified/atomization flow. Int. J. Multiphase Flow 23, 845–863.

Wasden, F.K., Dukler, A.E., 1989. Insights into the hydrodynamics of large wave interactions on free falling films. AIChE J. 35, 187–195.

Webb, R.L., 1994. Principles of Enhanced Heat Transfer. Wiley, London.

Yu, L.Q., Wasden, F.K., Dukler, A.E., Balakotaiah, V., 1995. Nonlinear evolution of waves on falling films at high Reynolds number. Phys. Fluids 7, 1886–1902.

Zabaras, G.J., 1985. Studies of vertical annular gas–liquid flows. Ph.D. Thesis in Chemical Engineering, University of Houston, Texas.

Zhang, J.T., Peng, X.F., Peterson, G.P., 2000. Experimental investigation on the hydrodynamics of falling liquid film flow by nonlinear description procedure. Int. J. Heat Mass Transfer 43, 3847–3852.